ISSN 0965-5441, Petroleum Chemistry, 2021, Vol. 61, No. 11, pp. 1234–1242. © Pleiades Publishing, Ltd., 2021.
ISSN 0965-5441, Petroleum Chemistry, 2021. © Pleiades Publishing, Ltd., 2021.
Russian Text © The Author(s), 2021, published in Neftekhimiya, 2021, Vol. 61, No. 6, pp. 827–837.

Non-Oxidative Conversion of Methane over a Mo/HZSM-5 Catalyst

Zh. B. Budaev[a,*], L. L. Korobitsyna[b], E. P. Meshcheryakov[a], I. A. Kurzina[a], and A. V. Vosmerikov[a,b,]**

[a] *Tomsk State University, Tomsk, 634050 Russia*
[b] *Institute of Petroleum Chemistry, Siberian Branch of Russian Academy of Sciences (IPC SB RAS), Tomsk, 634055 Russia*
**e-mail: budaev17@mail.ru; **e-mail: pika@ipc.tsc.ru*

Received July 9, 2021; revised July 22, 2021; accepted September 10, 2021

Abstract—The paper investigates the effects of an additional mesoporous structure on the physicochemical, textural, and catalytic properties of a Mo/HZSM-5 catalyst for methane dehydroaromatization. The mesoporous structure was generated by adding carbon black P354 during the synthesis of a ZSM-5 zeolite; this carbon was removed during the subsequent calcination of the sample. The catalyst consisted of 0.5–1.0 mm pellets that were prepared by molding a zeolite powder into tablets followed by their grinding and sifting through sieves. The paper describes the results of an investigation into the methane dehydroaromatization kinetics, as well as relevant data obtained by X-ray fluorescence, IR spectroscopy, X-ray diffraction, low-temperature nitrogen adsorption, transmission electron microscopy, and X-ray photoelectron spectroscopy. The addition of carbon black during the zeolite synthesis was demonstrated to improve the catalytic activity, with respect to aromatic production, and performance stability in non-oxidative methane conversion.

Keywords: methane, non-oxidative conversion of methane, zeolite, mesopores, carbon black

DOI: 10.1134/S0965544121110025

Although associated petroleum gas has a significantly lower content of methane than natural gas, the production of associated gas generally involves the incineration of methane and its homologues in flares. Therefore, it is very important to develop effective methods to process methane into valuable chemicals [1].

In 1993, Wang et al. [2] reported carrying out a reaction of methane dehydroaromatization (DHA) under non-oxidative conditions in a flow-through reactor using a molybdenum-modified ZSM-5 type zeolite. Compared to the oxidative process, the reducing environment resulted in a higher selectivity for the target benzene product.

Subsequently, a considerable number of studies have been performed in this area. These studies have used various transition metals as active components [3, 4], among which Mo has remained the most effective. The optimum Mo content in zeolite has been shown to be 2–6 wt % [5–7]. A wide range of supports have been investigated, and ZSM-5 has been identified as the most effective for the DHA process [7–10]. However, this zeolite has a number of drawbacks. In particular, narrow channels in its structure hinder mass transfer and increase coking, thus leading to the rapid deactivation of ZSM-5-based catalysts [11].

There are various methods for creating an additional mesoporous structure in a zeolite matrix. They mostly fall into two categories: direct synthesis with carbon materials (specifically, carbon and polymers) [12, 13], followed by their oxidation; and post-treatment of zeolite with various salts and alkalis [14, 15]. One of the simplest methods is the addition of carbon nanopowder to zeolite followed by annealing. This method requires neither additional conditions for the polymerization of the hydrocarbon template nor additional process steps for the synthesis.

In the present study, we utilized the first of the approaches mentioned above to generate an additional mesoporous structure. Specifically, to synthesize a ZSM-5

zeolite, we added a P354 grade carbon black, which was removed during the subsequent calcination of the sample.

The purpose of this study was to investigate the effects of the zeolite's mesoporous structure on the physicochemical and catalytic properties of the Mo/HZSM-5 catalyst in methane DHA.

EXPERIMENTAL

ZSM-5 high-silica zeolites with a SiO_2/Al_2O_3 molar ratio of 40 were prepared by hydrothermal crystallization from alkaline aluminosilicate gels [16], where water glass served as a source of silica. Hexamethylenediamine (HMDA) and carbon black C (P354 grade, manufactured by the Center of New Chemical Technologies BIC SB RAS, Omsk, Russia) were used as structure-directing agents. Crystallization was carried out in steel autoclaves with Teflon inserts at 175°C for three days. When the crystallization was completed, the solid phase was filtered from the liquid, washed with distilled water to remove excess alkali, and dried in air at 110°C for 8 h. To remove the HMDA and carbon, the samples were calcined in air at 550°C for 16 h. The zeolites were transformed into the active H-form by decationation with a 25% aqueous NH_4Cl solution at 90°C for 2 h, followed by washing with distilled water and calcination at 550°C for 6 h.

Mo/HZSM-5 catalysts were prepared by the dry mechanical mixing of the H-form of the synthetic zeolites with Mo nanopowder prepared by conductor electric explosion in an argon medium [17]. The mixing was carried out in a KM-1 ball vibratory mill for 2 h. The resultant mixtures were calcined in a muffle furnace in air at 550°C for 4 h.

The quality of the synthetic zeolites was monitored by IR spectroscopy and X-ray diffraction analysis (XRD). The IR spectra were recorded on a Nicolet 5700 spectrometer in the range of 4000–400 cm^{-1}. The zeolite crystallinity was measured by the method described in reference [18]. The state of molybdenum in the catalysts was detected by X-ray photoelectron spectroscopy (XPS) using a PHI VersaProbe II instrument. The Mo content in the samples was measured on a XRF-1800 sequential wavelength-dispersive X-ray fluorescence spectrometer. The phase composition and structural parameters of the samples were examined using a XRD-6000 diffractometer in CuK_α radiation. The PDF 4+ databases as well as the POWDER CELL 2.4 full-profile analysis software were used to determine the phase composition.

The zeolite morphology was examined using a JEOL JEM-2100F transmission electron microscope. To evaluate the porous structure parameters and the specific surface area, a TriStar II (3020) automated adsorption unit was used. The specific surface area was calculated from the low-temperature nitrogen adsorption isotherm (BET method). The acidic properties of the samples were examined by ammonia temperature-programmed desorption (NH_3–TPD), which enabled us to determine both the strength distribution and concentration of acid sites.

The non-oxidative conversion of methane (99.95 vol % purity) was carried out in a flow-through unit with a fixed catalyst bed at 750°C, atmospheric pressure, and a methane WHSV of 1000 h^{-1}. One 1.0 cm^3 of the catalyst was loaded into a tubular quartz reactor. The catalyst consisted of 0.5–1.0 mm pellets produced by molding the zeolite powder into tablets followed by their grinding and sifting through sieves. The reaction product was analyzed by GC using a Crystal 5000.2 chromatograph (Chromatec, Russia).

RESULTS AND DISCUSSION

To investigate the effects of the carbon template addition on the physicochemical and catalytic properties of Mo/HZSM-5 systems, a series of samples were prepared, some of them without carbon and others with the addition of 1.0 or 2.0 wt % of carbon black during the synthesis. The synthetic zeolites were then modified with molybdenum nanopowder in an amount of 4% by weight of the catalyst. The following samples were prepared and examined: HZSM-5; HZSM-5/1C; HZSM-5/2C (molybdenum-free samples); 4Mo/HZSM-5; 4Mo/HZSM-5/1C; and 4Mo/HZSM-5/2C (molybdenum-modified samples). Table 1 summarizes the main properties of the samples.

The tabular data clearly show that, with an increase in the amount of carbon added during the zeolite synthesis, the specific surface area slightly declined, the micropore volume remained roughly the same, and the mesopore volume increased by about 6–7%. Although the addition of molybdenum led to a drop in all the monitored parameters, the trends observed for the initial zeolite samples remained. Namely, the micropore volume did not change, and the mesopore volume grew by 6–9% with an increase in the carbon introduced.

The XRD patterns demonstrate that the positions and relative intensities of the reflections for all the samples

Table 1. Main properties of samples

Sample	Mo, wt %	S_{BET}, m^2/g	Total pore volume, cm^3/g	Mesopore volume, $cm^3/$	Micropore volume, cm^3/g	Average pore diameter, nm
HZSM-5	0.00	333	0.20	0.062	0.127	2.4
HZSM-5/1C	0.00	329	0.20	0.068	0.123	2.5
HZSM-5/2C	0.00	301	0.21	0.075	0.125	2.5
4Mo/HZSM-5	4.25	285	0.17	0.049	0.107	2.4
4Mo/HZSM-5/1C	4.29	293	0.18	0.056	0.109	2.4
4Mo/HZSM-5/2C	5.28	300	0.18	0.059	0.108	2.5

are identical to those for the ZSM-5 reference zeolite [19]. The XRD pattern does not depend on the amount of carbon used for the zeolite synthesis. Thus, the carbon addition did not affect the phase composition of the samples. An analysis of the XRD patterns suggests that the samples were well crystallized and contained no impurity phases. The coincidence in the relative positions of the main XRD peaks reflects the similarity of the crystalline structures of the samples synthesized. All the samples are classified as ZSM-5 rhombic structures. No characteristic peaks of molybdenum compounds were detectable in the XRD patterns of the molybdenum-modified samples due to insufficient Mo concentrations in the samples [20]. At low loads, no crystalline MoO_3 was detected, and Mo was amorphous.

The IR spectroscopy demonstrated (Fig. 1) an absorption band at 550–560 cm^{-1}, attributed to vibrations in the peripheral bonds of the $[SiO_4]$ and $[AlO_4]$ tetrahedra in the framework. This band is associated with the presence of four-membered, five-membered, and six-membered double rings, and plays a key role in the zeolite structure.

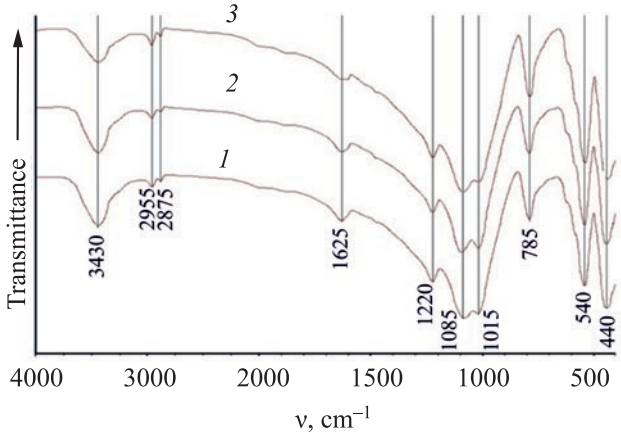

Fig. 1. IR spectra for: (*1*) HZSM-5; (*2*) HZSM-5/1C; and (*3*) HZSM-5/2C.

The crystallinity, estimated from the optical density ratio between the absorption bands at 550 cm^{-1} and 450 cm^{-1}, was equal to 100% for all the samples [18]. Therefore, despite the variety in structure-directing agents used for zeolite synthesis, all the samples synthesized were ZSM-5 type.

The molybdenum state in 4Mo/HZSM-5/1C was examined by transmission electron microscopy (TEM). Figure 2 shows a TEM micrograph for this sample as well as the distribution of chemical elements inside the particle.

The TEM images show no major presence of molybdenum oxide in the zeolite particle. The elemental MoL mapping indicates the relatively uniform distribution of molybdenum inside the zeolite. However, there are some areas of molybdenum localization corresponding to higher Mo concentrations, as evidenced by darker shadows in the bright-field image of the particle (Fig. 2e).

The regions of higher Mo concentration, as well as some randomly selected regions, were subjected to an elemental analysis to better understand the Mo distribution inside the zeolite (Table 2, Fig. 3).

The data of Table 2 confirm that the molybdenum concentration in the darker regions of the bright-field image is higher, as expected from Fig. 2. Thus, molybdenum is distributed throughout the catalyst without major aggregation. Despite the relatively uniform distribution of molybdenum, there are regions where molybdenum is localized in large amounts. This is likely associated with the catalyst preparation method.

The molybdenum state in the samples was further examined by XPS (Figs. 4a, 4b). The XPS spectra clearly show that molybdenum is present as a hexavalent oxide on the surface of all the samples.

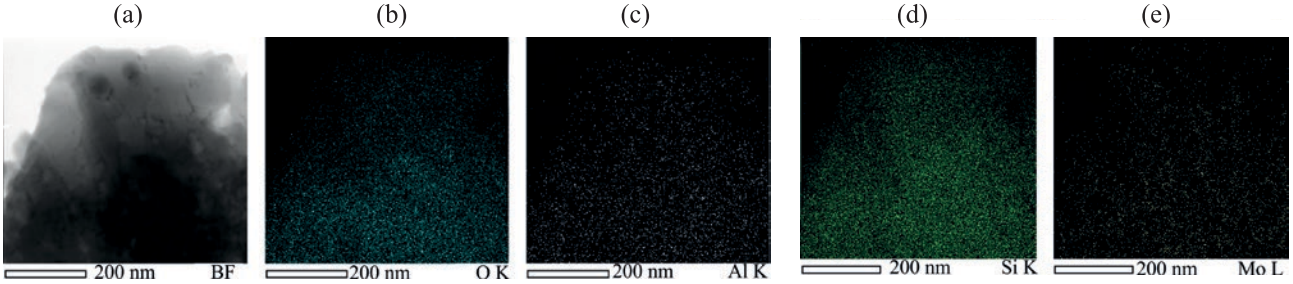

Fig. 2. (a) TEM micrograph for 4Mo/HZSM-5/1C catalyst particle; and distribution of (b) oxygen; (c) aluminum; (d) silicon; and (e) molybdenum inside the particle.

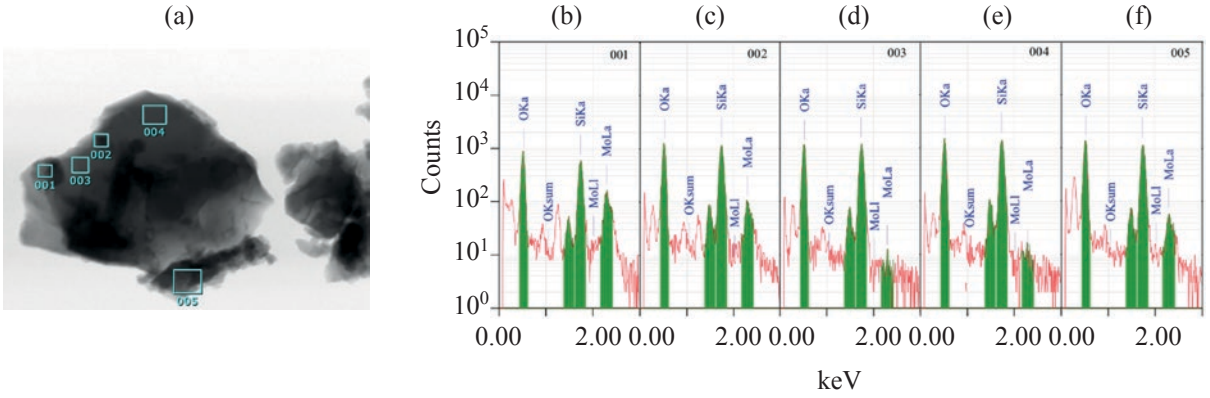

Fig. 3. (a) Elemental analysis regions; and spectra for the following regions: (b) 001; (c) 002; (d) 003; (e) 004; and (f) 005.

The molybdenum state inside the sample was estimated using layer-by-layer etching for seven minutes. When the etching procedure was completed, it was found that, although molybdenum was mostly contained in the form of MoO_3, MoO_2 was also present in the samples. The peak intensities indicate that the MoO_2 content declines with an increase in carbon addition. This suggests that molybdenum may not be fully oxidized during the catalyst synthesis. Instead, molybdenum located on the zeolite surface may be oxidized first, thus impeding any further metal oxidation in the bulk of the zeolite. Most probably, a higher addition of carbon nanopowder reduces the formation of MoO_2, and the newly-generated mesoporous structure provides better access to molybdenum inside the catalyst. Unfortunately, the measurement conditions hamper an accurate identification of silicon and aluminum structures in the samples.

Table 3 presents the molybdenum distribution inside the sample. Given the poor accuracy of the quantitative analysis of aluminum and oxygen due to the support's background effect, the distribution estimation was based on the molybdenum to silicon concentration ratio. The data for 4Mo/HZSM-5 clearly show a higher molybdenum

Table 2. Elemental composition in selected regions of 4Mo/HZSM-5/1C

Region	Mo, at %	Si, at %	Al, at %	O, at %
001	5.52	18.61	1.12	74.75
002	2.29	24.63	1.32	71.75
003	0.15	26.24	1.34	72.28
004	0.06	25.32	1.55	73.07
005	1.10	22.92	1.04	74.93

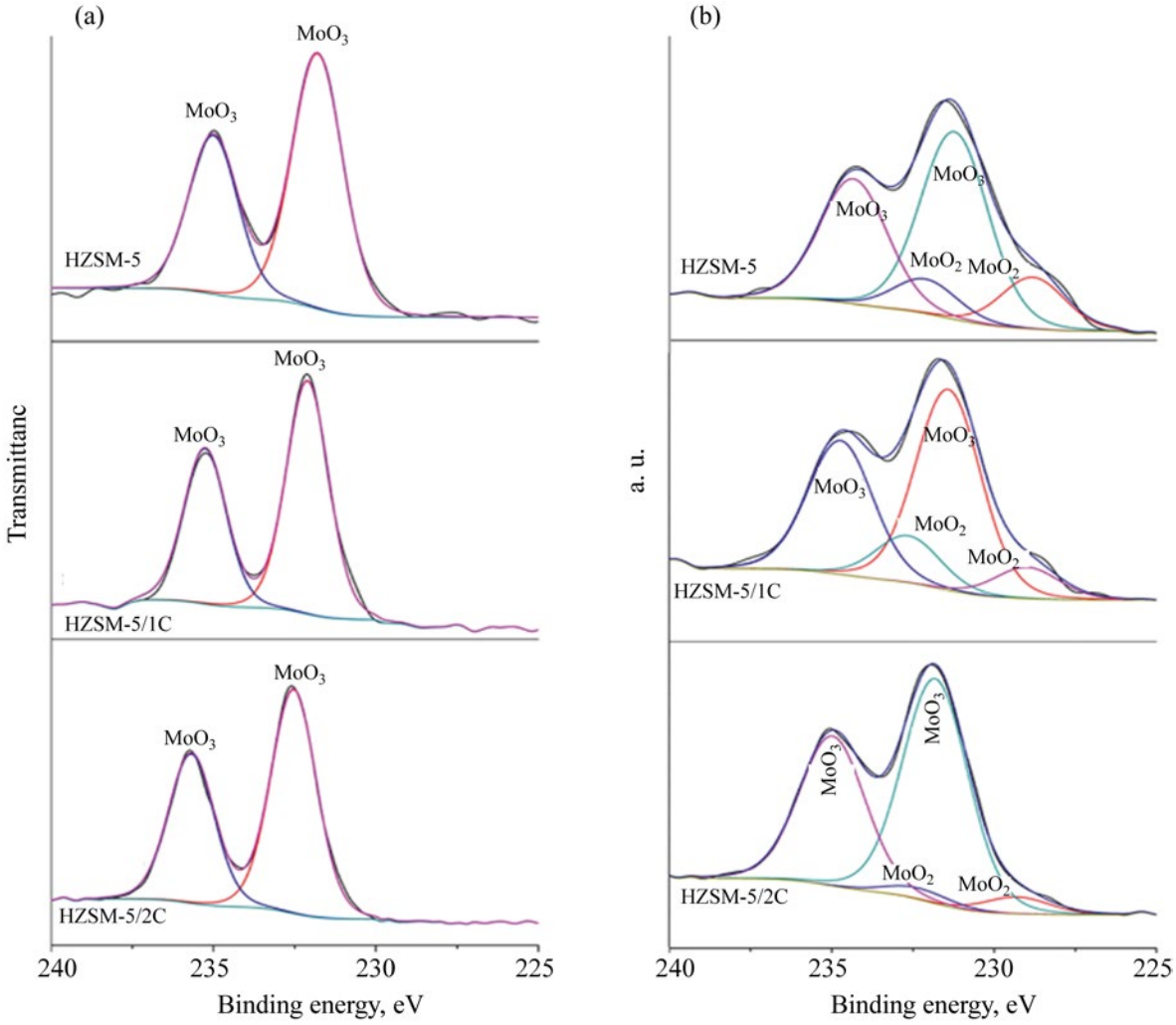

Fig. 4. XPS spectra of molybdenum oxide in samples: (a) outer bed; and (b) after layer-by-layer etching for 7 min.

concentration in the bulk than on the surface, which is indicative of a non-uniform molybdenum distribution.

An increase in the concentration of the carbon black introduced into the reaction mixture during the zeolite synthesis enhanced the uniformity of molybdenum distribution. This can be explained by the fact that the mesoporous structure improves the distribution of the molybdenum nanopowder inside the sample when mechanically mixed with the zeolite. The distribution becomes more uniform as the number of mesopores in the zeolite grows.

Table 4 summarizes the acidic properties of the zeolites synthesized both with and without the addition of various amounts of carbon black, as well as those of the respective Mo-containing catalysts.

Table 3. Molybdenum concentration in samples according to XPS

Sample	Mo/Si on surface	Mo/Si after etching
4Mo/HZSM-5	0.25	0.29
4Mo/HZSM-5/1C	0.43	0.44
4Mo/HZSM-5/2C	0.59	0.59

Table 4. Acidic properties of zeolites and catalysts based on them[a]

Sample	Temperature, °C		Concentration, μmol/g		
	T_I	T_{II}	C_I	C_{II}	C_Σ
HZSM-5	240	480	893	281	1174
HZSM-5/1C	240	480	636	280	916
HZSM-5/2C	240	480	635	254	889
4Mo/HZSM-5	200	470	703	278	981
4Mo/HZSM-5/1C	200	470	680	274	954
4Mo/HZSM-5/2C	200	470	617	229	846

[a] T_I and T_{II} are the maximum temperatures of low-temperature and high-temperature peaks, respectively; C_I and C_{II} are the concentrations of weak and strong acid sites, respectively; and C_Σ is the total concentration of acid sites.

The investigation of the acidic properties showed the presence of two acid site types in the initial zeolite: weak acid sites with an NH_3–TPD peak maximum at 240°C and strong acid sites with a peak maximum at 480°C. The total acid site concentration derived from the amount of desorbed ammonia was 1174 μmol/g (Table 4). The addition of 1.0 wt % of carbon black during the hydrothermal synthesis of zeolite reduced the concentration of weak acid sites, with no effect on their strength. The doubling of the carbon black concentration (to 2.0 wt %) had no major effect on the zeolite's acidic properties, except for some decline in the concentration of strong acid sites. The molybdenum modification of the zeolites shifted the peak maxima to lower temperatures in all cases. Furthermore, the concentration of low-temperature acid sites in 4Mo/HZSM-5 significantly declined when compared with the initial HZSM-5 zeolite. In contrast, the concentration of these sites in 4Mo/HZSM-5/1C (1.0 wt % carbon black added) grew in comparison with HZSM-5/1C, thus increasing the total concentration of acid sites in the zeolite. In the case of Mo modification of HZSM-5/2C, the concentrations of both acid site types declined.

Thus, all the samples under study contained acid sites of both types. The addition of carbon black during the zeolite synthesis reduced their concentration without changing their strength. 4Mo/HZSM-5 exhibited the highest concentration of acid sites among all the Mo-modified catalysts. The growth in the amount of carbon black reduced both the concentration of strong acid sites and the total acid site concentration. The differences in the acidic properties affected the catalytic properties of the samples in the non-oxidative conversion of methane to aromatics.

The data of the Mo/HZSM-5 catalytic tests in non-oxidative methane conversion are illustrated in Fig. 5. The highest methane conversion (12.1%) was observed for 4Mo/HZSM-5/2C, and the lowest (10.4%) for 4Mo/HZSM-5/1C.

On the other hand, 4Mo/HZSM-5/1C exhibited the highest performance stability throughout the test period. Specifically, after some deactivation in the initial 140 min of the reaction, its activity remained almost unchanged over the next 180 h. Although 4Mo/HZSM-5/2C achieved a higher conversion rate than 4Mo/HZSM-5 within the initial 20 min, its activity abruptly declined afterwards. The fact that 4Mo/HZSM-5/1C produced the highest stability was ensured by the optimum ratio between the numbers of weak and strong acid sites [21], and by the required ratio of micropore to mesopore volume in the catalyst

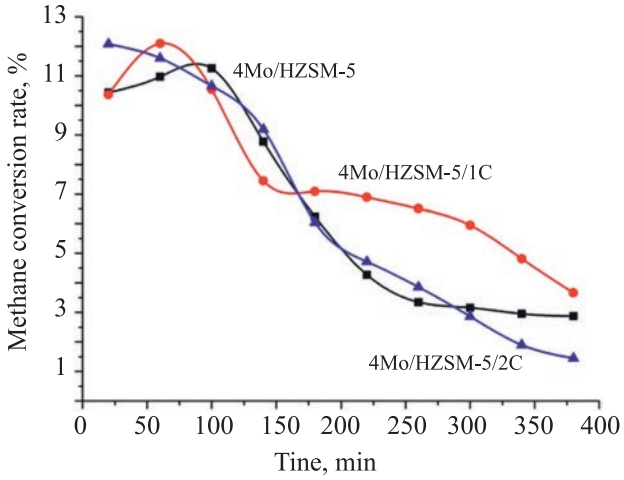

Fig. 5. Time variation in methane conversion rate for tested catalyst samples.

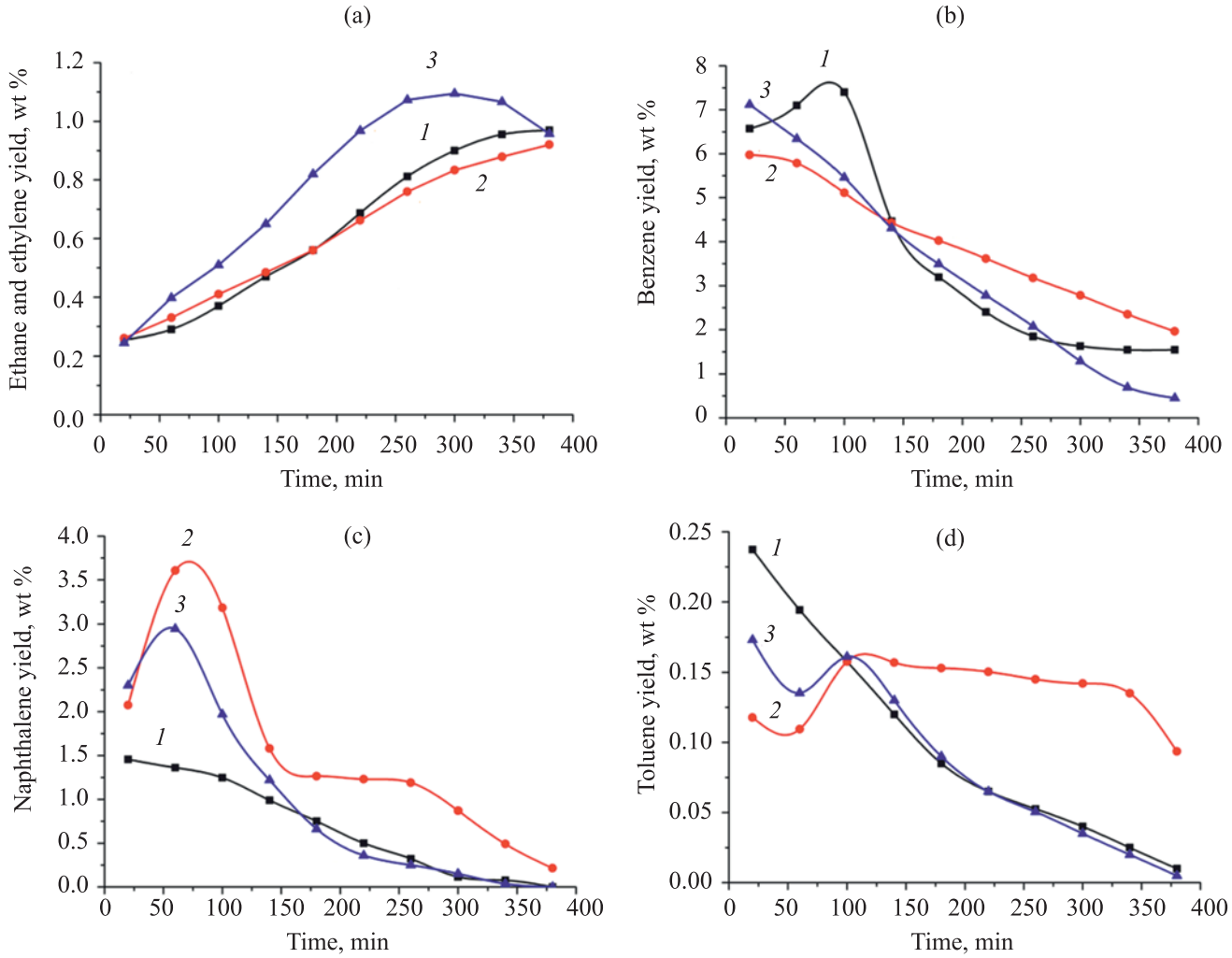

Fig. 6. Variations in the yields of (a) ethane and ethylene, (b) benzene, (c) naphthalene, and (d) toluene as functions of catalyst operation time in methane conversion: (*1*) 4Mo/HZSM-5; (*2*) 4Mo/HZSM-5/1C; and (*3*) 4Mo/HZSM-5/2C.

(Tables 1 and 4). Increasing the added carbon black to 2.0 wt % during the zeolite synthesis resulted in the formation of a relatively large number of mesopores, thus promoting the polycondensation of aromatics and coking. This is why 4Mo/HZSM-5/2C became less active more abruptly than the other samples.

Figure 6 illustrates the variations in the product yields as functions of the catalyst operation time.

According to the GC analysis, the gaseous products of methane conversion mostly consisted of ethane and ethylene. In addition, the gaseous phase contained hydrogen, unreacted methane, and—during the initial reaction period—small amounts of CO, CO_2, and H_2O. The yield of ethane and ethylene increased with the progress of the reaction, reaching a maximum after 300 min for 4Mo/HZSM-5/2C (Fig. 6a). For 4Mo/HZSM-5 and 4Mo/HZSM-5/1C, the total ethane/ethylene yield rose continuously up to the end of the test run, with 4Mo/HZSM-5/1C providing the lowest yield.

The highest amount of benzene was produced within the initial 100 min of the reaction over 4Mo/HZSM-5. For 4Mo/HZSM-5/2C, the highest benzene yield observed during the initial reaction period was followed by a decline over time, eventually falling below the benzene yield provided by 4Mo/HZSM-5. 4Mo/HZSM-5/1C produced the lowest amount of benzene among the three samples at the beginning of the reaction, but, because it had the slowest decline in benzene yield over the course of the reaction, this catalyst surpassed the other two from the 140th minute until the end of the test.

The naphthalene yield reached its maximum after 60 min of the reaction for the mesoporous samples, followed by a decline (Fig. 6c). The lowest naphthalene yield was observed for 4Mo/HZSM-5; this yield declined gradually and approached the naphthalene yield value provided by 4Mo/HZSM-5/2C after 140 min of the reaction. The highest yield of naphthalene was observed for 4Mo/HZSM-5/1C over almost the entire test run.

The toluene yield for 4Mo/HZSM-5 and 4Mo/HZSM-5/2C reached its maximum at the beginning of methane conversion, then declined, and virtually did not differ between these two samples after 100 min of the reaction (Fig. 6d). The highest yield of toluene after 100 min was produced with 4Mo/HZSM-5/1C, with a very minor variation over the following 240 min of the catalyst operation.

The above-mentioned differences in the catalytic activity and stability of the Mo-modified zeolite systems stem both from their respective acidic properties and from the size and morphology of their zeolite crystals. The initial zeolite particles are fairly homogeneous in composition and appear as 6–8 μm polycrystalline spheroids. With an increase in the amount of carbon added during zeolite synthesis, the crystals become more heterogeneous, with particles larger in size (up to 12 μm) and often structurally different from the initial zeolite particles [22, 23].

The more abrupt decline in the catalytic activity of 4Mo/HZSM-5/2C, compared with 4Mo/HZSM-5/1C, may be due to its relatively high activity in the initial period, resulting in a more rapid carbonization and deactivation of the catalyst. The best properties in methane DHA were demonstrated by 4Mo/HZSM-5/1C. This catalyst maintained a high methane conversion rate throughout the test run, with a much slower decline than for the other samples. In addition, this catalyst ensured the lowest yield of ethane and ethylene and the highest yield of the target aromatic product.

CONCLUSIONS

This article describes an investigation of the effects of the addition of carbon black during zeolite synthesis on the physicochemical and catalytic properties of both the initial zeolites and a number of Mo/HZSM-5 catalysts prepared from the zeolites with and without the addition of carbon black. It was demonstrated that the addition of carbon to the reaction mixture during the synthesis does not affect the crystallinity and phase composition of the synthetic zeolites, but does increase the mesopore volume in the catalyst. Based on the analysis of the acidic properties of the catalysts, zeolite modification with molybdenum was shown to reduce the number of acid sites. The initial HZSM-5 zeolite and the 4Mo/HZSM-5 catalyst were found to contain the highest numbers of acid sites, and 4Mo/HZSM-5/2C to have the lowest. The catalytic properties of the Mo-modified catalysts are significantly affected by the properties of the initial zeolites synthesized with different amounts of carbon black added. 4Mo/HZSM-5/1C showed the highest activity and performance stability in methane dehydroaromatization. Thus, the formation of mesopores in zeolite resulting from the introduction of carbon black as a secondary template during the synthesis produces a catalyst that exhibits a higher activity and performance stability without significant effects on its structure and textural properties.

AUTHOR INFORMATION

Zh.B. Budaev, ORCID: https://orcid.org/0000-0001-7539-7282

L.L. Korobitsyna, ORCID: https://orcid.org/0000-0003-1679-483X

E.P. Meshcheryakov, ORCID: https://orcid.org/0000-0002-4490-1308

I.A. Kurzina, ORCID: https://orcid.org/0000-0003-4976-2295

A.V. Vosmerikov, ORCID: https://orcid.org/0000-0002-7569-0902

ACKNOWLEDGMENTS

The authors are grateful to Dr. Aleksandr Chernyavskii, Lead Engineer of the Russian Technological University (RTU MIREA), for his kind cooperation in the examinations for the study.

FUNDING

This work was carried out with support from the Ministry of Sciences and Higher Education of the Russian Federation (project no. 0721-2020-0037) and within the state assignment for IPC SB RAS funded by the Ministry of Sciences and Higher Education of the Russian Federation.

CONFLICT OF INTEREST

The authors declare no conflict of interest requiring disclosure in this article.

REFERENCES

1. Corredor, E.C., Chitta, P., and Deo, M.D., *Fuel Proc. Technol*., 2019, vol. 183, pp. 55–61. https://doi.org/10.1016/j.fuproc.2018.05.038
2. Wang, L., Tao, L., Xie, M., and Xu, G., *Catal. Lett*., 1993, vol. 21, no. 1, pp. 35–41. https://doi.org/10.1007/BF00767368
3. Weskhuysen, B.M., Wang, D., Rosynek, M.P., and Lunsford, J.H., *J. Catal*., 1998, vol. 175, pp. 338–346.
4. Wu, Y., Holdren, C., Zhang, Y., Oh, S.C., Tran, D.T., Emdadi, L., and Lu, Z., *J. Catal*., 2019, vol. 372, pp. 128–141. https://doi.org/10.1016/j.jcat.2019.02.024
5. Ma, D., Shu, Y., Han, X., Liu, X., Xu, Y., and Bao, X., *J. Phys. Chem. B*, 2001, vol. 105, no. 9, pp. 1786–1793. https://doi.org/10.1021/jp002011k
6. Chen, L., Lin, L., Xu, Z., and Li, Zh.T., *J. Catal*., 1995, vol. 157, no. 1, pp. 190–200.
7. Korobitsyna, L.L., Kozlov, V.V., and Vosmerikov, A.V., *Izv. Tomsk. Politekh. Univ.: Khim. Khim. Tekhnol*., 2014, vol. 325, no. 3, pp. 71–79.
8. Chen, L., Lin, L., Xu, Z., Li, X., and Zhang, T., *J. Catal*., 1995, vol. 157, no. 1, pp. 190–200.
9. Xu, Y., Liu, S., Guo, X., Wang, L., and Xie, M., *Catal. Lett*., 1995, vol. 30, pp. 135–149. https://doi.org/10.1007/BF00813680
10. Solymosi, F., Csereny, A., Szoke, A., Bansagi, T., and Oszko, A., *J. Catal*., 1997, vol. 165, no. 2, pp. 150–161. https://doi.org/10.1006/JCAT.1997.1478
11. Rahman, M., Infantes-Molina, A., Boubnov, A., Bare, S.R., Stavitski, E., Sridhar, A., and Khatib, Sh.J., *J. Catal*., 2019, vol. 375, no. 1, pp. 314–328. https://doi.org/10.1016/j.jcat.2019.06.002
12. Hu, T., Liu, J., Cao, Ch., and Song, W., *Chinese J. Catal*., 2017, vol. 38, no. 5, pp. 872–877. https://doi.org/10.1016/S1872-2067(17)62828-6
13. Kuvatova, R.Z., Travkina, O.S., and Kutepov, B.I., *Katal. Prom–ti*, 2020, vol. 20, no. 5, pp. 328–334. https://doi.org/10.18412/1816-0387-2020-5-328-334
14. Schmidt, I., Christensen, C.H., Hasselriis, P., Kustova, M.Yu., Brorson, M., Dahl, S., Johannsen, K., and Christensen, C.H., *Stud. Surface Sci. Catal*., 2005, vol. 154, pp. 1247–1254. https://doi.org/10.1016/S0167-2991(05)80471-9
15. Christensen, C.H., Johannsen, K., and Schmid, I., *J. Am. Chem. Soc*., 2003, vol. 125, no. 44, pp. 13370–13371. https://doi.org/10.1021/ja037063c
16. Velichkina, L.M., Korobitsyna, L.L., and Vosmerikov, A.V., *Neftepererab. Neftekhim*., 2005, no. 10, pp. 32–35.
17. Gusev, A.I., *Nanokristallicheskie materialy: metody polucheniya i svoistva* (Nanocrystalline Materials: Production Methods and Properties), Yekaterinburg: Ural. Otd. Ross. Akad. Nauk, 1988.
18. Shukla, D.B. and Pandya, V.P., *J. Chem. Tech. Biotechnol*., 1989, no. 44, pp. 147–154.
19. Breck, D.W., *Zeolite Molecular Sieves*, New York: Wiley, 1974.
20. Ramasubramanian, V., Ramsurn, H., and Price, G.L., *J. Energy Chem*., 2019, vol. 34, pp. 20–32. https://doi.org/10.1016/j.jechem.2018.09.018
21. Wu, Y., Emdadi, L., Schulman, E., Shu, Y., Tran, D.T., Wang, X., and Liu, D., *Micropor. Mesopor. Mater*., 2018, vol. 263, pp. 1–10. https://doi.org/10.1016/j.micromeso.2017.11.040
22. Korobitsyna, L.L., Zharnov, K.N., Stepanov, A.A., and Vosmerikov, A.V., *J. Sib. Fed. Univ.: Chem*., 2019, vol. 12, no. 1, pp. 118–125. https://doi.org/10.17516/1998-2836-0111
23. Yang, L., Liu, Zh., Liu, Zh., Peng, W., Liu, Y., and Liu, Ch., *Chinese J. Catal*., 2017, vol. 38, no. 4, pp. 683–690. https://doi.org/10.1016/S1872-2067